Investigation of the Energetic Performance of Pure Silica ITQ-4 (IFR) Zeolite under High Pressure Water Intrusion

ARTICLE *in* THE JOURNAL OF PHYSICAL CHEMISTRY C · JUNE 2010

Impact Factor: 4.77 · DOI: 10.1021/jp102663f

6 AUTHORS, INCLUDING:

Mohamed Ali Saada

16 PUBLICATIONS **145** CITATIONS

SEE PROFILE

Séverinne Rigolet

Institut de Science des Matériaux de Mulho…

85 PUBLICATIONS **765** CITATIONS

SEE PROFILE

J.-L. Paillaud

French National Centre for Scientific Resea…

122 PUBLICATIONS **1,353** CITATIONS

SEE PROFILE

Nicolas Bats

IFP Energies nouvelles

60 PUBLICATIONS **1,208** CITATIONS

SEE PROFILE

Investigation of the Energetic Performance of Pure Silica ITQ-4 (IFR) Zeolite under High Pressure Water Intrusion

Mohamed Ali Saada,[†] Séverinne Rigolet,[†] Jean-Louis Paillaud,[†] Nicolas Bats,[‡] Michel Soulard,[†] and Joël Patarin*,[†]

Equipe Matériaux à Porosité Contrôlée (MPC), Institut de Science des Matériaux de Mulhouse (IS2M), LRC CNRS 7228, Université de Haute Alsace, ENSCMu, 3 Rue Alfred Werner, 68093 Mulhouse, France, and IFP-Lyon, Rond-Point de l'Échangeur de Solaize, B.P. 3, 69360 Solaize, France

Received: March 24, 2010; Revised Manuscript Received: May 27, 2010

To study the energetic performance of the 1D 12-membred-ring pure silica ITQ-4 zeolite (IFR topology), a high-pressure water intrusion−extrusion isotherm at room temperature was performed. The pressure−volume diagram indicates an irreversible phenomenon, water molecules remaining confined in ITQ-4 micropores. Therefore, the "water−ITQ-4" system appears to behave as a bumper. The water intrusion pressure and intruded volume are of 42 MPa and 0.136 mL/g, respectively. Investigations on the ITQ-4 samples by ^{29}Si and ^{1}H solid-state NMR spectroscopy and powder X-ray diffraction have confirmed the existence of a small amount of silanol defects in the nonintruded sample and an increase of these defects after the water intrusion−extrusion experiment. It appears clearly that one of the crystallographic silicon sites of the porous framework is particularly affected after such a treatment, leading to the creation of Si−OH groups by the breaking of siloxane bonds, these silanols being strongly hydrogen bonded with water molecules.

1. Introduction

In the past decade, thermodynamics of confined systems involving water as nonwetting liquid and hydrophobic porous solid have attracted considerable attention due to their potential application in the field of energetics.[1,2] Gusev[3] and Eroshenko and Fadeev[4] have reported the discovery of this feature in the mid-1990s, following the investigation of heterogeneous systems made of water and silica gels. An extension to the functionalized organized mesoporous[5−7] and pure silica zeolites (zeosils)[1,8] was achieved later. Various zeosil materials, such as MFI,[1] *BEA,[2] DDR,[2] FER,[9] and CHA[10,11] were tested as water confining microporous matrices. Only some of them were considered as good candidates for energy storage.[11,12] Simultaneously to the experimental approach, great attention has been paid to the theoretical study of the water confined behavior by computer modeling[13−19] in order to get new insights into the various factors involved in the water intrusion−extrusion phenomenon.

Zeosils are known as being hydrophobic materials.[20] To penetrate water in such microporous matrices, a certain pressure must be applied.[21] During this forced penetration (intrusion), the resulting mechanical energy can be converted into an interfacial one. Indeed, the massive water is transformed into a multitude of molecular clusters developing a large zeosil−water interface. From a microscopic point of view, this fact can be explained by the breaking of intermolecular bonds in the water to create new bonds with the microporous zeosils. When the pressure is released, the system can evolve spontaneously by expelling water out of the cavities of the zeosil (extrusion) with a more or less significant hysteresis.[22] Consequently, the system allows accumulating and restoring significant amounts of energy.

Diverse behaviors illustrated by pressure−volume diagrams can be observed depending on various physicochemical and topological parameters related to the porous framework such as hydrophobic/hydrophilic character, pore size and type (cages or channels), and channels dimensionality (1D, 2D, or 3D). According to phenomenon reversibility or irreversibility, the water−zeosils systems are able to restore, partly absorb, or completely dissipate mechanical energy. Consequently, molecular spring, shock-absorber, or bumper behaviors can be observed.[1,2,8,17]

A water intrusion process has been applied to several zeosil materials with accessible pore opening. It was shown that the pure silica chabazite (Si−CHA) material having large cages with eight-membered ring (MR) openings acts as a molecular spring displaying a reversible water intrusion−extrusion isotherm with a pronounced hysteresis in the relax stage.[10] The purely siliceous DDR-type zeolite containing also 8-MR apertures presents an almost similar pressure−volume diagram.[2,23] The silicalite-1 (MFI topology), which is a 10-membered-ring pure silica zeolite, proved to behave as a molecular spring with an intrusion pressure around 100 MPa and an amount of stored energy about 10 J/(g of zeolite).[24] For the 12-membered-ring *BEA zeosil, which consists of at least two polytypes, the water intrusion process is irreversible and no energy can be restored. The presence of defect sites at the interface of the two polytypes could explain its bumper behavior.[2]

The purpose of this work is to assess the energetic performance, using a water intrusion−extrusion experiment, of the 1D microporous pure silica ITQ-4 material. This porous silica polymorph (IFR topology) is characterized by a large sinusoidal 12-MR channel (window size, 6.2 Å × 7.2 Å) parallel to the *c*-axis crystallographic direction in the monoclinic space group *C*2/*m*.[25−27] Thanks to its large void and pore aperture, such a topology appears to have potential applications in catalysis. Indeed, its Al-containing form was found to be an effective material for the hydroisomerization of short *n*-alkane chains and

* To whom correspondence should be addressed. E-mail: joel.patarin@uha.fr.
[†] Université de Haute Alsace.
[‡] IFP-Lyon.

10.1021/jp102663f
Published on Web 06/10/2010

for the reforming of C_7-C_{10} normal parafins.[28] The energetic performance of the pure silica ITQ-4 zeolite remains unknown. To highlight this aspect, a study on a microcrystalline sample was carried out to investigate its behavior regarding the water intrusion−extrusion process. The ITQ-4 samples were fully characterized mainly by powder X-ray diffraction (PXRD) using the Rietveld method, ^{29}Si and ^{1}H solid-state NMR spectroscopies, scanning electron microscopy (SEM), N_2 adsorption−desorption, and thermal analysis. All these multiscale techniques were performed before and/or after water intrusion in order to give further clarifications of the involved phenomena, particularly on the existence of silanol defects.

2. Experimental Section

2.1. Sample Preparation. The synthesis of pure silica ITQ-4 sample was performed hydrothermally in the presence of fluoride anions using *N*-benzylquinuclidinium cations as the organic structure-directing agent according to the procedure described by Barrett et al.[26] The resulting crystalline product was washed with demineralized water after filtration and dried at 80 °C overnight. Calcination was then carried out at 580 °C in air for 15 h in order to liberate completely the porosity.

2.2. Scanning Electron Microscopy. The morphology and size of the ITQ-4 crystals were examined by SEM before and after the water intrusion process using a Philips XL30 microscope equipped with a field electron gun. Prior to the SEM observations, all samples were coated with gold.

2.3. Powder X-ray Diffraction. The PXRD patterns of both ITQ-4 samples (with calcination and after intrusion−extrusion of water) were collected on a PANalytical MPD X'Pert Pro diffractometer in a Debye−Scherrer geometry equipped with a capillary sample holder, a hybrid mirror monochromator (λ = 1.5406 Å) which gives the monochromatic parallel beam geometry, and a X'Celerator real-time multiple strip detector (active length = 2.122° (2θ)). The powders were introduced in Mark tubes made of special glass (no. 14; outside diameter, 0.3 mm; Hilgenberg Gmbh), and then the filled capillary tubes were mounted on a precise goniometric head which is screwed on a rotary sample stage; the spinning rate was 1 Hz. The powder patterns were collected at 295 K in the range of 7° < 2θ < 90°, with step = 0.008° 2θ and time/step = 3155 s, and the total collecting time was about 64 h. The PXRD pattern of calcined ITQ-4 was indexed with the expected monoclinic unit cell parameters in space group *C*2/*m* (No. 12), a = 18.6273(1) Å, b = 13.4895(8) Å, c = 7.6276(5) Å, β = 101.619(4)°, and V = 1877.3(2) Å^3 (after refinement, $F(30)$ = 200.5), by the Louër's DICVOL91 indexing routine[29] of the STOE WinX^{POW} program package.[30] After intrusion−extrusion of water the refined unit cell parameters are a = 18.6058(1) Å, b = 13.4945(9) Å, c = 7.6073(7) Å, β = 101.434(6)°, and V = 1872.1(3) Å^3 ($F(30)$ = 157.7). The Rietveld refinement was performed using the GSAS package.[31] All the atoms were refined isotropically; soft restraints were placed on the bond lengths and angles of the framework (T−O = 1.60(4) Å and O−T−O = 109.5(40)°). After refinement of the framework, successive calculated Fourier difference maps revealed scattering densities inside the void volume attributed to the presence of adsorbed water molecules. Then, oxygen atoms were placed on these positions and refined (positions and occupancy factors). Further details on crystallographic and Rietveld refinement data are given in Table 1. The final atomic parameters are listed in Table 2. In Tables 3 and 4 bond distances and selected bond angles are reported, respectively. CIF files are also available as Supporting Information.

TABLE 1: Rietveld Refinement Data of the Calcined and Intruded−Extruded ITQ-4 Samples

		intruded−extruded
chemical name	calcined ITQ-4	ITQ-4
chemical formula (asymmetric unit)	$Si_4O_{8.248}$[a]	$Si_4O_{9.092}$[a]
calcd formula weight (g/mol)	243.89	257.81
space group	*C*2/*m* (no. 12)	
a (Å)	18.6386(1)	18.6046(2)
b (Å)	13.4948(1)	13.4947(1)
c (Å)	7.6305(1)	7.6075(1)
β (deg)	101.616(1)	101.425(1)
V (Å^3)	1879.94(2)	1872.11(4)
Z	8	8
density(calcd) (g.cm^{-3})	1.726	1.829
no. of contributing reflections	820	851
no. of structural parameters	64	61
no. of profile parameters	18	18
total no. of restraints (Si−O, ⟨O−Si−O⟩)[b]	16, 24	16, 24
total no. of constraints	2[c]	2[c]
R_p[d]	0.0518	0.0396
wR_p[d]	0.0660	0.0466
wR_{exp}[e]	0.0532	0.0512
R_F[e]	0.0397	0.0603
R_F^2[e]	0.0615	0.0907
χ^2[e]	1.537	1.047
largest diff peak and hole (e Å^{-3})	0.379, −0.365	0.641, −0.820

[a] In the chemical formulas are considered the sum of the oxygen atoms of the framework and water molecules as listed in Table 2. The Rietveld refinement did not take into account the scattering power of the hydrogen atoms of each water molecule. Consequently, the true number of water molecules should be about 25% lower than the s.o. factor refined for these oxygen atoms. [b] Si−O = 1.60(4) Å; ⟨O−Si−O⟩ = 109.5(40)°. [c] In a first step, the thermal parameter of the Si, framework oxygen, and water oxygen atoms were constrained to be equal. Then the thermal parameter constraint applied on the Si atoms was removed (see Results and Discussion). [d]

$$R_p = \sum\{[|y_o - y_c||y_o - y_b|/y_o]/\sum|y_o - y_b|\}$$

$$wR_p = \{\sum[w(y_o - y_c)(y_o - y_b)/y_o]^2/\sum[w(y_o - y_b)^2]\}^{1/2}$$

where y_o, y_c, and y_b are y observed, y calculated, and y background, respectively. [e] The definition of these residual values are given in ref 31a.

2.4. N_2 Adsorption−Desorption Measurements. Nitrogen sorption isotherms were carried out on a Micromeritics ASAP 2420 apparatus at liquid nitrogen temperature (−196 °C). Prior to the measurement, the calcined ITQ-4 sample was outgassed in situ under vacuum at 300 °C overnight (15 h). The specific surface area (S_{BET}) and microporous volume (V_{micro}) were calculated using the BET and *t*-plot methods, respectively.

2.5. Thermal Analysis. The thermal behavior of the pure silica ITQ-4 samples (≈20 mg) before and after water intrusion−extrusion experiment was investigated by means of thermogravimetric analysis (TGA) using a Setaram Sensys evo TG apparatus with a heating rate of 5 °C/min up to 750 °C under a flow of nitrogen−oxygen mixture.

2.6. Water Intrusion−Extrusion Experiments. According to the procedure described in ref 10, a modified mercury porosimeter (Micromeritics Model Autopore IV) was used to perform the water intrusion−extrusion experiments on the calcined pure silica ITQ-4 sample. The solid and water weights were of 0.45 and 0.75 g, respectively. The experimental pressure−volume diagram is obtained after subtraction of the

TABLE 2: Atomic Coordinates, Site Occupancy, and Equivalent Isotropic Displacement Parameters for Calcined and Intruded−Extruded ITQ-4 Samples (Standard Deviations in Parentheses)

atoms	multiplicity and Wyckoff letters	sof	*x/a*	*y/b*	*z/c*	*U* (Å^2)
		Calcined ITQ-4 Samples				
Si1	8j	1	0.48782(15)	0.38647(22)	0.69742(34)	0.0163(9)
Si2	8j	1	0.25297(15)	0.38537(21)	0.3771(4)	0.0168(9)
Si3	8j	1	0.64698(14)	0.38407(21)	0.9011(4)	0.018(1)
Si4	8j	1	0.33935(15)	0.29798(21)	0.7303(4)	0.0196(9)
O1	8j	1	0.42423(26)	0.3141(4)	0.7326(8)	0.0178(6)
O2	4h	1	1/2	0.3718(6)	1/2	0.0178(6)
O3	8j	1	0.56144(27)	0.3585(4)	0.8379(7)	0.0178(6)
O4	4i	1	0.4625(4)	1/2	0.7217(10)	0.0178(6)
O5	8j	1	0.31781(26)	0.1841(4)	0.6790(8)	0.0178(6)
O6	8j	1	0.28992(28)	0.3685(4)	0.5850(7)	0.0178(6)
O7	8j	1	0.32140(27)	0.3208(4)	0.9228(6)	0.0178(6)
O8	4i	1	0.6568(4)	1/2	0.9511(10)	0.0178(6)
O9	8j	1	0.68917(28)	0.35908(35)	0.7443(7)	0.0178(6)
O10	4i	1	0.2271(4)	1/2	0.3482(10)	0.0178(6)
Ow1	8j	0.051(7)	0.347(7)	0.043(12)	0.125(19)	0.15(5)
Ow2	8j	0.061(9)	−0.0919(29)	0.2753(33)	0.428(7)	0.15(5)
Ow3	8j	0.045(7)	0.386(9)	0.094(12)	0.367(27)	0.15(5)
Ow4/OH	4i	0.078(11)	−0.0488(28)	0	0.013(5)	0.15(5)
Ow5	4i	0.062(11)	0.481(11)	0	0.715(29)	0.15(5)
Ow6	4i	0.041(12)	0.536(18)	0	−0.06(5)	0.15(5)
		Intruded−Extruded ITQ-4 Samples				
Si1	8j	1	0.48677(24)	0.38594(30)	0.6973(5)	0.0118(16)
Si2	8j	1	0.25243(23)	0.38687(33)	0.3810(7)	0.0102(15)
Si3	8j	1	0.64679(26)	0.3790(4)	0.8984(7)	0.0384(20)
Si4	8j	1	0.33867(24)	0.29626(34)	0.7309(7)	0.0179(17)
O1	8j	1	0.4229(4)	0.3134(6)	0.7305(12)	0.0116(9)
O2	4h	1	1/2	0.3724(9)	1/2	0.0116(9)
O3	8j	1	0.5600(4)	0.3584(6)	0.8321(11)	0.0116(9)
O4	4i	1	0.4651(6)	1/2	0.7320(16)	0.0116(9)
O5	8j	1	0.3177(4)	0.1811(5)	0.6808(12)	0.0116(9)
O6	8j	1	0.2894(4)	0.3665(6)	0.587(1)	0.0116(9)
O7	8j	1	0.3219(4)	0.3201(6)	0.9190(11)	0.0116(9)
O8	4i	1	0.6564(6)	1/2	0.9449(16)	0.0116(9)
O9	8j	1	0.6901(4)	0.3587(6)	0.7389(10)	0.0116(9)
O10	4i	1	0.2239(6)	1/2	0.3528(15)	0.0116(9)
Ow1	8j	0.332(14)	0.4394(23)	0.105(4)	0.082(6)	0.268(27)
Ow2/OH	8j	0.297(18)	−0.1343(29)	0.243(5)	0.188(8)	0.268(27)
Ow3	8j	0.200(32)	0.485(7)	0.084(9)	0.605(14)	0.268(27)
Ow4	4i	0.369(16)	0.3385(31)	0	0.260(8)	0.268(27)
Ow5	4i	0.16(6)	0.525(11)	0	1.29(4)	0.268(27)

curve corresponding to the compressibility of pure water. Pressure is expressed in megapascals (MPa), and the volume variation in milliliters (mL) per gram of anhydrous calcined sample. The values of intrusion (P_{int}) and extrusion (P_{ext}) pressure correspond to the half-volume total variation. The experimental error is estimated to 1% on the pressure and on the volume.

2.7. Solid-State NMR Spectroscopy. ^{29}Si ($I = 1/2$) magic angle spinning (MAS) and ^{1}H−^{29}Si cross-polarization magic angle spinning (CPMAS) NMR spectra were recorded, at room temperature, with a Bruker double-channel 7 mm probe with a spinning frequency of 4 kHz, on a Bruker Avance II 400 spectrometer operating at $B_0 = 9.4$ T (Larmor frequency, $\nu_0(^{29}\text{Si}) = 79.49$ MHz and $\nu_0(^1\text{H}) = 400.13$ MHz). ^{29}Si single-pulse MAS NMR experiments were performed with a $\pi/6$ pulse duration of 2.65 μs and a 80 s recycling delay. These recording conditions ensure the quantitative determination of the proportions of the different Q_n Si species.[32] ^{1}H−^{29}Si CPMAS NMR experiments were acquired using a ramp for Hartmann−Hahn matching with a ^{1}H $\pi/2$ pulse duration of 7.9 μs and a contact time of 5 ms. The radiofrequency field strength used for ^{1}H decoupling was set to 60.9 kHz.

^{1}H ($I = 1/2$) MAS NMR experiments were performed at room temperature on a Bruker Avance II 400 spectrometer operating at $B_0 = 9.4$ T (Larmor frequency, $\nu_0 = 400.13$ MHz). To identify the different types of proton present in the ITQ-4 material, the samples under study must be dehydrated in order to remove the water which prevents the observation of the hydrogen species. The procedure allowing the elimination of physisorbed water but avoiding dehydroxylation reactions consists of heating the ITQ-4 samples at 50 °C overnight under a reduced pressure of ∼3 Pa. The dehydrated samples are then transferred into a glovebox and packed in the 2.5 mm rotor under dry argon. Single-pulse experiments were recorded with a double-channel 2.5 mm Bruker MAS probe, a spinning frequency of 30 kHz, and a $\pi/2$ pulse duration of 3.85 μs. ^{1}H spin−lattice relaxation times (T_1) were measured with the inversion−recovery pulse sequence for all samples. Typically, 600 scans were recorded.

^{1}H−^{29}Si heteronuclear correlation (HETCOR) experiment was performed at room temperature, with a Bruker double-channel 4 mm probe, on a Bruker Avance II 400 spectrometer operating at $B_0 = 9.4$ T (Larmor frequency, $\nu_0(^{29}\text{Si}) = 79.49$ MHz and $\nu_0(^1\text{H}) = 400.13$ MHz), using a ramp for Hartmann−Hahn matching with a spinning frequency of 14 kHz, a ^{1}H $\pi/2$ pulse duration of 5.9 μs, and a contact time of 1 ms. Chemical shifts reported thereafter are relative to tetramethylsilane for both ^{1}H and ^{29}Si nuclei. Decompositions of the spectra were performed using the Dmfit software.[33]

TABLE 3: Bond Lengths (Å) for Calcined and Intruded−Extruded ITQ-4 Samples and Closest Contacts between Water and Framework Oxygen Atoms (Standard Deviations in Parentheses)

calcined ITQ-4			intruded−extruded ITQ-4		
Si1	O2	1.580(3)	Si1	O3	1.579(8)
	O1	1.600(6)		O2	1.579(4)
	O3	1.607(5)		O1	1.598(9)
	O4	1.625(4)		O4	1.626(6)
Si2	O9	1.597(7)	Si2	O9	1.583(9)
	O5	1.605(6)		O5	1.588(8)
	O6	1.613(6)		O6	1.606(9)
	O10	1.622(4)		O10	1.617(6)
Si3	O9	1.595(7)	Si3	O7	1.606(9)
	O7	1.601(5)		O9	1.608(10)
	O3	1.608(6)		O3	1.618(9)
	O8	1.612(3)		O8	1.673(6)
Si4	O1	1.594(6)	Si4	O7	1.557(10)
	O7	1.601(6)		O1	1.585(9)
	O6	1.604(6)		O6	1.594(9)
	O5	1.616(6)		O5	1.629(8)
		⟨1.605⟩			⟨1.603⟩
Ow4	O8	2.09(5)	Si3	Ow2	1.77(7)
	O3	2.26(2)	Ow2	O9	1.87(6)
	O3	2.26(2)		O3	1.97(6)
	O4	2.27(4)		O7	2.22(6)
	O4	2.32(4)			

TABLE 4: Bond Angles (Å) for Calcined and Intruded−Extruded ITQ-4 Samples (Standard Deviations in Parentheses)

calcined ITQ-4				intruded−extruded ITQ-4			
Si1	O2	O1	109.7(3)	Si1	O3	O2	108.3(4)
	O2	O3	109.8(2)		O3	O1	109.0(5)
	O2	O4	109.1(2)		O3	O4	109.1(4)
	O1	O3	107.9(3)		O2	O1	109.9(4)
	O1	O4	108.3(3)		O2	O4	110.7(2)
	O3	O4	112.0(3)		O1	O4	109.8(4)
Si2	O9	O5	109.3(3)	Si2	O9	O5	107.5(5)
	O9	O6	109.6(3)		O9	O6	108.3(5)
	O9	O10	110.5(2)		O9	O10	113.1(4)
	O5	O6	110.2(3)		O5	O6	111.0(5)
	O5	O10	108.4(3)		O5	O10	106.1(4)
	O6	O10	109.0(3)		O6	O10	110.9(4)
Si3	O9	O7	111.3(3)	Si3	O7	O9	114.7(5)
	O9	O3	109.8(3)		O7	O3	110.7(5)
	O9	O8	109.5(2)		O7	O8	107.2(4)
	O7	O3	108.2(3)		O9	O3	110.7(5)
	O7	O8	108.3(3)		O9	O8	106.1(4)
	O3	O8	109.7(2)		O3	O8	107.0(4)
Si4	O1	O7	110.7(3)	Si4	O7	O1	110.5(5)
	O1	O6	110.9(3)		O7	O6	108.4(5)
	O1	O5	109.3(3)		O7	O5	109.3(5)
	O7	O6	108.9(3)		O1	O6	110.3(5)
	O7	O5	108.5(3)		O1	O5	109.3(5)
	O6	O5	108.5(3)		O6	O5	109.2(5)
			⟨109.5⟩				⟨109.5⟩

3. Results and Discussion

3.1. XRD Results. As it will be seen below (section 3.7, Structure Analysis), the high-resolution powder XRD patterns of the ITQ-4 samples before and after the water intrusion−extrusion experiment attest that the crystallinity of the sample decreases after the intrusion of water, indicating a slight collapse of the structure subsequently to such a treatment.

3.2. Scanning Electron Microscopy. The scanning electron micrographs of the calcined ITQ-4 sample before water intrusion are given in Figure 1a. The crystals display truncated prismatic morphology with a size ranging from 3 to 11 μm. After water intrusion under high pressure, the aspect of the crystals is completely changed. The SEM picture (Figure 1b) reveals a major destruction of the ITQ-4 crystals contrary to what is observed for pure silica MFI[9] and CHA[11] topologies, where no significant change is observed after water intrusion−extrusion experiments.

3.3. N_2 Adsorption−Desorption Isotherms. Figure 2 illustrates the N_2 adsorption−desorption isotherms of the calcined ITQ-4 sample before the water intrusion−extrusion experiment. The isotherm is of type I and characteristic of microporous solid. The associated Brunauer−Emmett−Teller (BET) surface area is of 646 m^2/g. Its relatively large value is related to the large microporous volume, which is equal to 0.23 mL/g. Such a value is similar to that of the *BEA type zeolite; both zeosils displaying 12-MR pore openings.

3.4. Water Intrusion−Extrusion Isotherms. The pressure−volume diagram of the "water−ITQ-4" system is given in Figure 3. The intrusion curve presents an important variation of volume exemplified by a relatively extended step; its associated height corresponds to the intruded water volume in the zeolite micropores ($V_{int.}$ = 0.136 mL/g). However, this volume is far away from the one determined from N_2 adsorption measurements (i.e., 0.23 mL/g). As it was shown by Desbiens et al.[14,34] for silicalite-1, the value of the intruded volume determined for a water density of 1 has to be corrected since the average computed water density in the MFI structure is around 0.6 g/mL. Taken also into account this correction for the ITQ-4 sample, the intruded volume is thus totally consistent with the pore volume determined from nitrogen adsorption data, i.e., ∼0.25 mL/g. The water intrusion pressure (P_{int}) is found to be of 45 MPa. Finally, after a complete filling of the micropores, a classical compression of the water−ITQ-4 system takes place. When the pressure is released, the system is irreversible. The intruded water is not expelled and remains confined in the microporous matrix. Consequently, the water−ITQ-4 system is able to dissipate the amount of energy stored during the compression stage and acts as a bumper. A bumper behavior was already observed in the case of *BEA type zeolite.[2,23] As it will be shown by powder X-ray diffraction analysis and NMR spectroscopy, the bumper behavior of the water−ITQ-4 system is probably due to the increase of the amount of silanol defects in the zeolite framework after the water intrusion step.

3.5. Thermogravimetric Analysis. The experimental results issued from the thermogravimetric (TG) analysis of the pure silica ITQ-4 samples before and after the water intrusion−extrusion experiment are depicted in Figure 4a,b, respectively. Both samples were placed in a controlled saturated atmosphere of 85 wt % water for 48 h. According to Figure 4a, the weight loss of the calcined ITQ-4 sample occurs in two steps. The first one (1.8 wt %) takes place under 100 °C and may be ascribed to the desorption of physisorbed water molecules. It represents about two molecules of water per unit cell. The second weight loss (∼0.8 wt %) which occurs in the temperature range of 100−500 °C with a main step around 350 °C could correspond to the removal of traces of water trapped in the micropores or arising from dehydroxylation reactions. After the water intrusion−extrusion experiment (Figure 4b) the TG curve presents three weight losses. The first one (5.5 wt % at 180 °C) corresponds to the removal of water sequestered in the porous framework (about 6 molecules of water/(unit cell)). A second lower weight loss (∼1 wt %) takes place between 180 and 400 °C; it is due possibly to water molecules in stronger interaction with the inorganic framework. A third and final weight loss

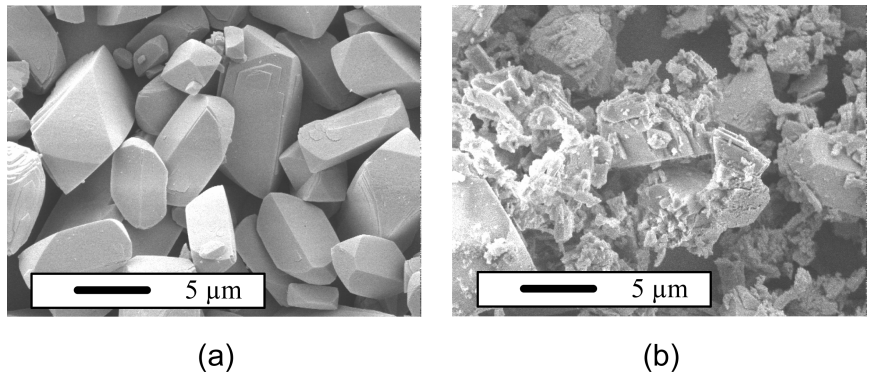

Figure 1. SEM images of calcined ITQ-4 samples: (a) before and (b) after intrusion−extrusion of water.

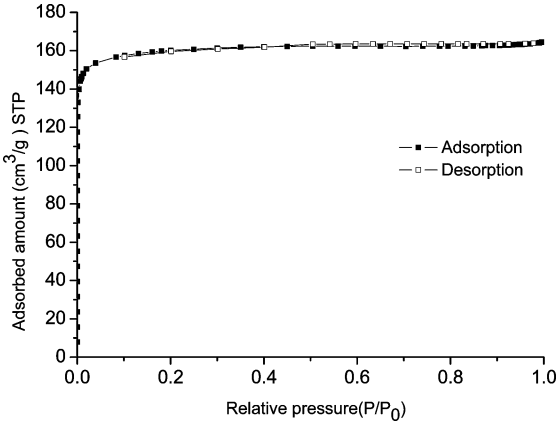

Figure 2. N_2 adsorption−desorption isotherms of calcined ITQ-4 sample.

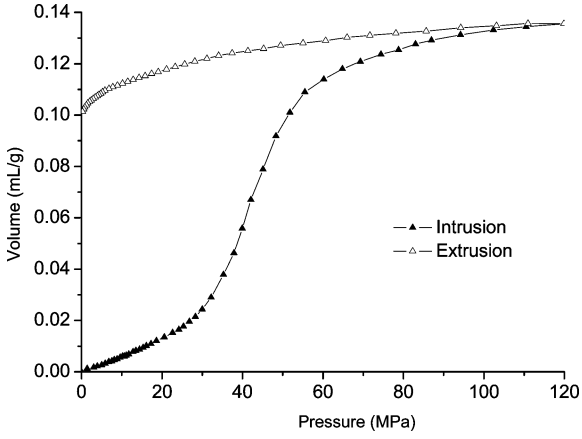

Figure 3. Pressure−volume diagram of the water−ITQ-4 system at room temperature.

(∼1 wt %) occurs at temperatures above 400 °C and is ascribed to the elimination of water arising from dehydroxylation reactions.

The thermal analysis study shows clearly that the hydrophobic/hydrophilic character of the ITQ-4 sample completely changed after the water intrusion−extrusion experiment, and, in agreement with the XRD and SEM results, part of the inorganic framework has been very affected after such a treatment.

3.6. Solid-State NMR Investigations. ***^{29}Si MAS NMR.*** The highly resolved ^{29}Si MAS NMR spectra of ITQ-4 samples and their deconvolution are reported in Figure 5 and Table 5. The spectrum of the starting material (calcined sample, Figure 5a) exhibits four thin resonances assigned to the four crystallographically inequivalent silicon sites and is associated with Q_4 groups (Si−(OSi)$_4$). A small broad peak accounting for 3% of

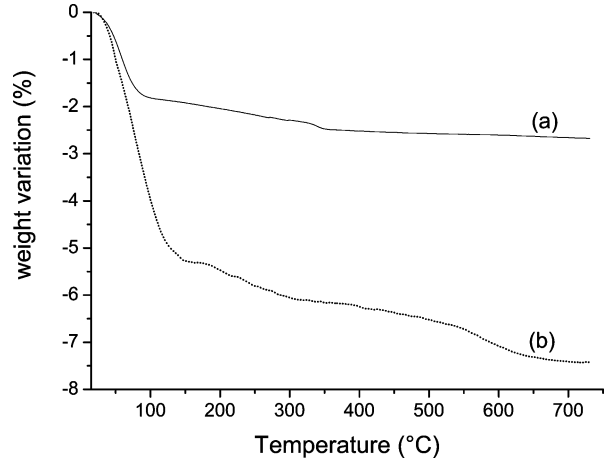

Figure 4. TG curves of calcined ITQ-4 samples: (a) before and (b) after intrusion−extrusion of water.

the total ^{29}Si signal is also detected at −100.7 ppm and can be assigned to Q_3 groups (HO−Si−(OSi)$_3$). After the water intrusion−extrusion experiment, a new resonance at −101.3 ppm (Figure 5b) appears, proving that about 5% (Table 5) of new Q_3 sites were created during such a treatment. Furthermore, the increase of defects results in the broadening of all Q_4 sites (see half-height widths in Table 5), indicating a decrease of the local structural order of the inorganic framework. With a particular attention to the proportion of different sites (Table 5), it is very interesting to note that the site located at −107.1 ppm decreases remarkably (from 24 to 16%). This suggests that this silicon site is mainly responsible of the appearance of new Q_3 silanols; the latter arising from the breaking of siloxane bonds (≡Si−O−Si≡) under high water pressure.

^{1}H−^{29}Si CPMAS NMR. The ^{1}H−^{29}Si CPMAS NMR spectra of the ITQ-4 samples before and after intrusion−extrusion of water (Figure 6) were performed in order to enhance the silicon atoms that bear protons and thus to get evidence of the presence of silanol groups. Although the CPMAS technique does not provide quantitative results, it is possible to make a relative comparison of the spectra if they were registered under the same conditions. Such experiments evidence the presence of a weak broad resonance at around −92 ppm corresponding to Q_2 species ((HOSi)$_2$−(OSi)$_2$) for both samples which is not affected by water intrusion. The spectral area assigned to Q_3 species shows the presence of at least four types of silanols for the nonintruded sample. This result could mean that in the pure silica ITQ-4 material all of the four inequivalent crystallographic sites present silanol Q_3 defects. More interesting after water intrusion, the resonance located at −101.3 ppm is particularly exalted, which tends to prove that this silicon site is preferentially affected

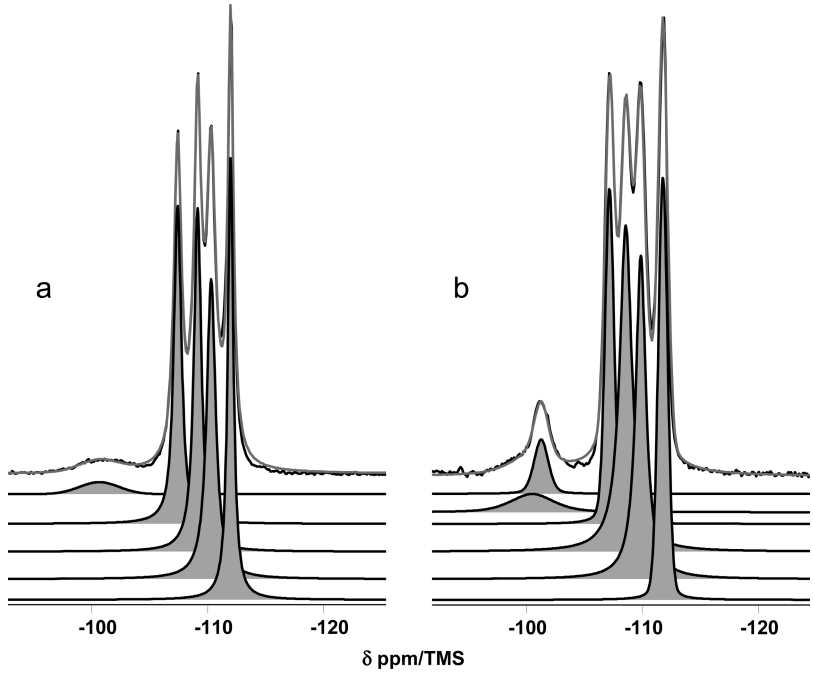

Figure 5. ^{29}Si MAS NMR spectra of calcined ITQ-4 samples: (a) before and (b) after intrusion−extrusion of water with their decomposition.

TABLE 5: ^{29}Si Chemical Shift and Amount (%) of the Silicon Species Estimated from the MAS Spectra of the ITQ-4 Samples before and after Intrusion−Extrusion of Water

	calcined			intruded−extruded		
MAS	δ (ppm)	half-height width	%	δ (ppm)	half-height width	%
Q_4	−111.9	0.6	22	−111.8	1.5	21
	−110.3	0.9	25	−109.9	1.1	26
	−109.1	0.8	26	−108.5	1.3	29
	−107.4	0.8	24	−107.1	0.9	16
Q_3	−100.7	4.0	3	−101.3	1.5	4
				−100.5	4.4	5

during water intrusion. In the Q_4 area, the intensity of the four resonances previously described by the ^{29}Si MAS technique increases after water intrusion, which reveals that the local environment of these sites was enriched in proton in SiOH or/and water molecules form.

^{1}H MAS NMR. The ^{1}H MAS NMR spectra of ITQ-4 material before and after intrusion−extrusion of water are displayed in Figure 7. The samples were dehydrated (50 °C, 3 Pa) to remove the ^{1}H signal from physisorbed water molecules as much as possible. After decomposition of the signals, it appears that the spectra consist of 15 resonances that can be grouped into three areas. The first, between 0 and 2.5 ppm, is usually assigned to isolated and geminal silanol groups ((≡Si−OH), (=Si(OH)$_2$)).[35] The second area ranging from 2.5 to 5 ppm corresponds to silanols hydrogen bonded to water as already observed in Si−CHA[11] or mesoporous materials.[36] Finally, between 5 and 8 ppm, the signals are attributed to liquidlike physisorbed water molecules.[37] What is important to note when comparing both spectra is that, after intrusion−extrusion of water, the spectrum is dominated by the resonance at 2.2 ppm. It corroborates the observations made by ^{29}Si NMR: under high water pressure, some specific silanols (signal at −101.3 ppm, Figure 6) are formed after the breaking of siloxane bridges.

^{1}H−^{29}Si CP HETCOR. To highlight the specificity of these new silanols created by water intrusion, a two-dimensional ^{1}H−^{29}Si CP HETCOR experiment (Figure 8) correlating the

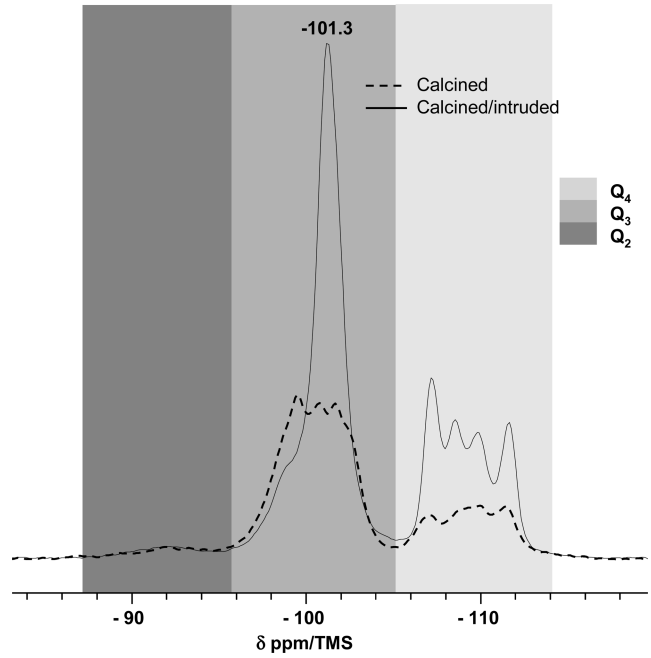

Figure 6. ^{1}H→^{29}Si CPMAS NMR spectra of calcined ITQ-4 samples: before (--) and after (—) intrusion−extrusion of water.

^{1}H isotropic spectrum to neighboring ^{29}Si was performed on the dehydrated (50 °C/∼3 Pa) intruded ITQ-4 sample. The cross-section corresponding to Q_3 indicates that the proton of the silanol species at 2.2 ppm correlates mainly with the silicate resonance at −101.3 ppm. The ^{1}H−^{29}Si CP HETCOR spectrum provides evidence of the proximity between this proton and this type of silicon, and therefore they form the same entity Si−OH.

3.7. Structure Analysis. The Rietveld plots of calcined ITQ-4 before and after intrusion−extrusion of water (Figure 9) show a long-range order of the IFR structure. However, as described above, the powder pattern of the intruded and extruded sample highlights a lowering of the crystallinity. The intensities are lower, and the plot of the full width at half-maximum (fwhm) extracted from the Rietveld refinement versus the diffraction

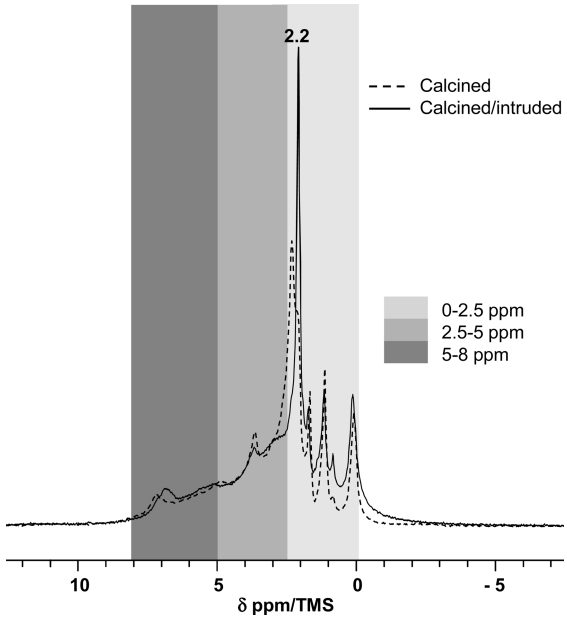

Figure 7. ^{1}H MAS NMR spectra of calcined ITQ-4 samples before (--) and after (—) water intrusion−extrusion of water and soft dehydration.

angles (Figure 10) proves that the reflections of calcined ITQ-4 are sharper than those of the intruded−extruded product. The unit cell parameters of both materials are similar (Table 1), and the average Si−O bonds (1.605 Å; Table 3) and ⟨O−Si−O⟩ angles (109.5°; Table 4) are characteristic of Si atoms in a tetrahedrally coordinated environment.

Due to the crystallographic disorder, the total amount of extraframework oxygen atoms located during the Rietveld refinement is lower than the one determined by the thermogravimetric study. Indeed, from the site occupancy factors of the extraframework oxygen atoms listed in Table 2, there are the equivalent of about 1.5 and 6.5 molecules of water/(unit cell) of calcined and intruded−extruded ITQ-4 samples, respectively, instead of 2.9 and 8.7 as determined from the TG analysis.

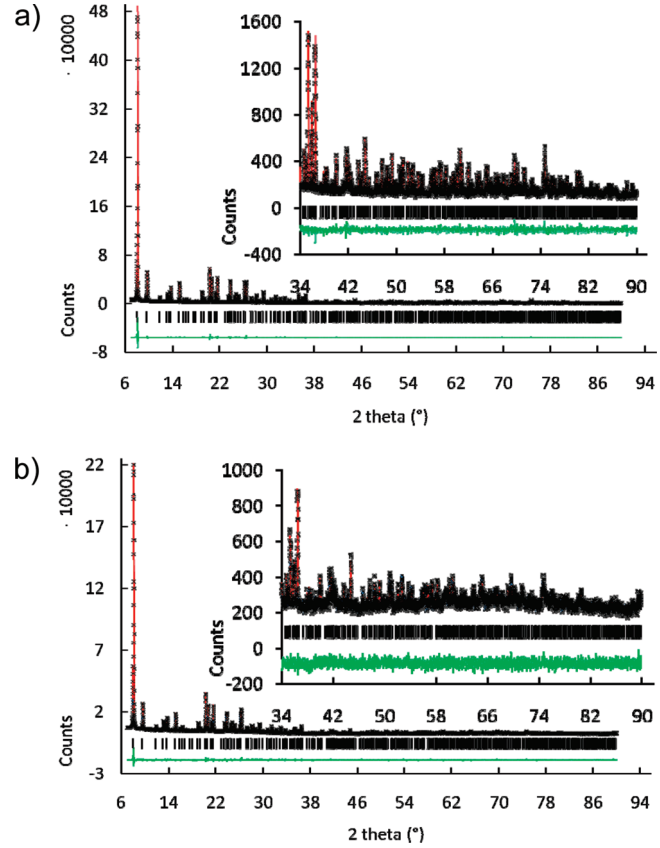

Figure 9. Rietveld plots of calcined ITQ-4 samples (a) before and (b) after intrusion−extrusion of water, experimental (×) and simulated (−) powder XRD patterns. Vertical ticks indicate the positions of the theoretical reflections for space group *C*2/*m*. The lowest trace is the difference plot.

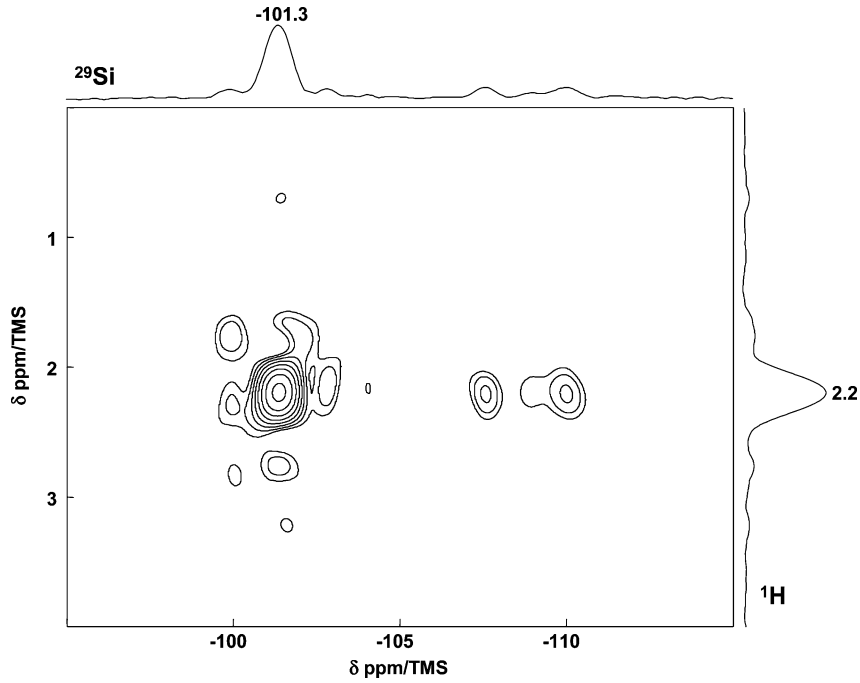

Figure 8. Two-dimensional ^{1}H−^{29}Si CP HETCOR NMR spectrum of the calcined ITQ-4 sample after intrusion−extrusion of water and soft dehydration.

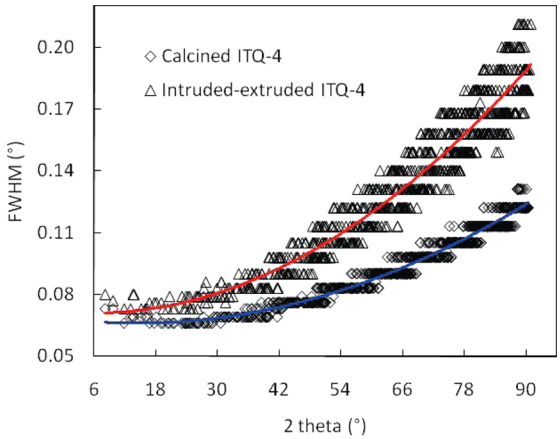

Figure 10. Fwhm of the reflections extracted from the Rietveld refinements of calcined and intruded−extruded ITQ-4 samples.

After location of the adsorbed water molecules for both products, the temperature factors of the silicon atoms were refined independently in order to detect eventual defects around some particular Si atoms for which an increase of the thermal parameters may be expected. From Table 2, the temperature factor values of the silicon atoms obtained for the calcined ITQ-4 sample are centered on 0.0177 Å^2 with a low standard deviation of 0.0015 Å^2. The situation is quite different after intrusion−extrusion of water; the corresponding mean value of 0.0196 Å^2 is slightly higher, but the standard deviation is about 10 times higher (0.013 Å^2) and the silicon Si3 (0.0384(20) Å^2) is more than twice warmer than Si1, Si2, and Si4. Moreover, the oxygen atom found inside the composite building unit *lau* or [4^{2}6^4]-a cage (Ow4/OH in Figure 11a) is too close to the framework oxygen atoms O3, O4, and O8 connected to Si3 (see the distances in Table 3) to be consider as a water molecule; it reflects more the presence of a small amount of disordered silanol groups around the crystallographic site Si3. For this reason we called it Ow4/OH. After intrusion−extrusion of water, a similar situation is observed but in this case; the oxygen atom named Ow2/OH close to Si3 is certainly part of a silanol group that dangles in the 12-MR channels (Figure 11b).

From the present Rietveld analysis, in spite of the lack of precision on the true location of the species around Si3, it is possible to assign the Q_3 resonance located at −101.3 ppm in the ^{1}H→^{29}Si CPMAS NMR spectrum to silicon Si3 (Figure 6). The observed intensity decrease after the water intrusion of the Q_4 resonance at −107,1 ppm in the ^{29}Si MAS spectrum (Figure 5) allows us to assign also that resonance to silicon Si3.

4. Conclusion

The pure silica ITQ-4 zeolite performance toward a water intrusion−extrusion process reveals a bumper behavior. Before intrusion, the presence of a small amount of silanol defects is proved by ^{29}Si and ^{1}H MAS NMR spectroscopy in agreement with the TG data. ^{1}H MAS NMR together with the TG data also show that a small amount of adsorbed water is already present in the 12-MR channels after calcination due to the hydrophilic character of the silanol defects inside the structure. Upon intrusion−extrusion of water, NMR results indicate the creation of additional Si−OH groups (Q_3), arising mainly from one of the four crystallographically inequivalent silicon sites (Q_4) by the breaking of siloxane (Si−O−Si) bonds under high water pressure. Water molecules are not expelled from the rather hydrophobic pure silica ITQ-4 zeolite after the intrusion−extrusion of water. The Rietveld refinement confirms the presence of silanol defects before and after intrusion, and it was possible to assign the additional silanol Q_3 groups to the crystallographic silicon site Si3.

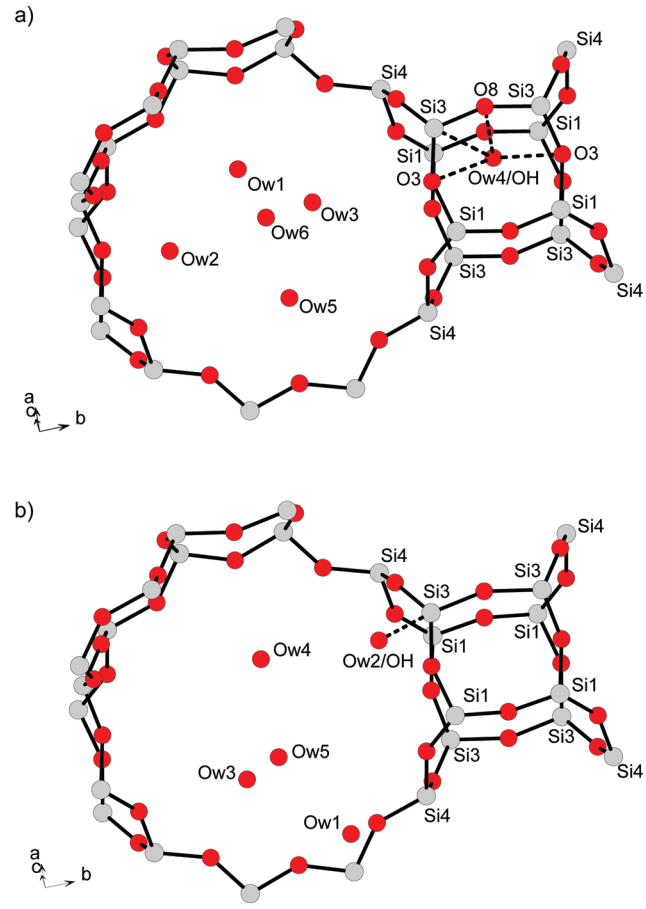

Figure 11. Projection of ITQ-4 structures: (a) before and (b) after intrusion−extrusion of water showing the water molecules inside the straight channels and the short distances between framework and extraframework oxygen atoms near the silicon site Si3. The site occupancy factors (sof) of the Ow atoms are five times higher for the intruded−extruded sample (see Table 2).

Acknowledgment. This work was supported by the French Agence Nationale de la Recherche through the ANR program "Heter-eau", under Contract No. BLAN 06-3_144027.

Supporting Information Available: Additional information contained in two CIF files. This material is available free of charge via the Internet at http://pubs.acs.org.

References and Notes

(1) Eroshenko, V.; Regis, R. C.; Soulard, M.; Patarin, J. *J. Am. Chem. Soc.* **2001**, *123*, 8129.

(2) Soulard, M.; Patarin, J.; Eroshenko, V.; Regis, R. C. In *Recent Advances in the Science and Technology of Zeolites and Related Materials: Proceedings of the 14th International Zeolite Conference*; Van Steen, E., Callanan, L., Claeys, M., Eds.; Studies in Surface Science and Catalysis 154; Elsevier B.V.: Amsterdam, 2004; p 1830.

(3) Gusev, V. Y. *Langmuir* **1994**, *10*, 10.

(4) Eroshenko, V. A.; Fadeev, A. Y. *Colloid J.* **1995**, *57*, 446.

(5) Martin, T.; Lefevre, B.; Brunel, D.; Galarneau, A.; Di Renzo, F.; Fajula, F.; Gobin, P. F.; Quinson, J. F.; Vigier, G. J. *Chem. Commun. (Cambridge, U. K.)* **2002**, 24.

(6) Lefevre, B.; Saugey, A.; Barrat, J. L.; Bocquet, L.; Charlaix, E.; Gobin, P. F.; Vigier, G. J. *J. Chem. Phys.* **2004**, *120*, 4927.

(7) Coiffard, L.; Eroshenko, V. A.; Grolier, J.-P. E. *AIChE J.* **2005**, *51*, 1246.

(8) Eroshenko, V.; Regis, R. C.; Soulard, M.; Patarin, J. *C. R. Phys.* **2002**, *3*, 111.
(9) Trzpit, M.; Soulard, M.; Patarin, J.; Desbiens, N.; Cailliez, F.; Boutin, A.; Demachy, I.; Fuchs, A. H. *Langmuir* **2007**, *23*, 10131.
(10) Trzpit, M.; Soulard, M.; Patarin, J. *Chem. Lett.* **2007**, *36*, 980.
(11) Trzpit, M.; Rigolet, S.; Paillaud, J.-L.; Marichal, C.; Soulard, M.; Patarin, J. *J. Phys. Chem. B* **2008**, *112*, 7257.
(12) Trzpit, M.; Soulard, M.; Patarin, J. *Microporous Mesoporous Mater.* **2009**, *117*, 627.
(13) Demontis, P.; Stara, G.; Suffritti, G. B. *J. Phys. Chem. B* **2003**, *107*, 4426.
(14) Desbiens, N.; Boutin, A.; Demachy, I. *J. Phys. Chem. B* **2005**, *109*, 24071.
(15) Cailliez, F.; Trzpit, M.; Soulard, M.; Demachy, I.; Boutin, A.; Patarin, J.; Fuchs, A. H. *Phys. Chem. Chem. Phys.* **2008**, *10*, 4817.
(16) Coudert, F.-X.; Cailliez, F.; Vuilleumier, R.; Fuchs, A. H.; Boutin, A. *Faraday Discuss.* **2009**, *141*, 377.
(17) Cailliez, F.; Boutin, A.; Demachy, I.; Fuchs, A. H. *Mol. Simul.* **2009**, *35*, 24.
(18) Pellenq, R. J.-M.; Roussel, T.; Puibasset, J. *Adsorption* **2008**, *14*, 733.
(19) Özgür Yazaydin, A.; Thompson, R. W. *Microporous Mesoporous Mater.* **2009**, *123*, 169.
(20) Caullet, P.; Paillaud, J. L.; Simon-Masseron, A.; Soulard, M.; Patarin, J. *C. R. Chim.* **2005**, *8*, 245.
(21) Washburn, R. W. *Proc. Natl. Acad. Sci. U.S.A.* **1921**, *7*, 115.
(22) Denoyel, R.; Beurroies, I.; Lefevre, B. *J. Pet. Sci. Eng.* **2004**, *45*, 203.
(23) Trzpit, M. *Thesis*, University of Haute-Alsace, Mulhouse, France, 2008.
(24) Trzpit, M.; Soulard, M.; Patarin, J. *J. Mater. Sci.* **2009**, *44*, 6525.
(25) Camblor, M. A.; Corma, A.; Villaescusa, L. A. *Chem. Commun. (Cambridge, U. K.)* **1997**, 749.
(26) Barrett, P. A.; Camblor, M. A.; Corma, A.; Jones, R. H.; Villaescusa, L. A. *J. Phys. Chem. B* **1998**, *102*, 4147.
(27) Villaescusa, L. A.; Barrett, P. A.; Kalwei, M.; Koller, H.; Camblor, M. A. *Chem. Mater.* **2001**, *13*, 2332.
(28) Barrett, P. A.; Camblor, M. A.; Corma, A.; Jones, R. H.; Villaescusa, L. A. *Chem. Mater.* **1997**, *9*, 1713.
(29) Boultif, A.; Louër, D. *J. Appl. Crystallogr.* **1991**, *24*, 987.
(30) *STOE WinX^{POW}*; Version 1.06; STOE and Cie GmbH: Darmstadt, Germany, 1999.
(31) (a) Larson, A. C.; Von Dreele, R. B. *General Structure Analysis System*; Los Alamos National Laboratory Report LAUR 86-748; Los Alamos National Laboratory: Los Alamos, NM, 2000. (b) Toby, B. H. *J. Appl. Crystallogr.* **2001**, *34*, 210.
(32) Engelhardt, G.; Michel, D. *High-Resolution Solid State NMR of Silicates and Zeolites*; John Wiley & Sons: Chichester, U.K., 1987.
(33) Massiot, D.; Fayon, F.; Capron, M.; King, I.; Le Calvé, S.; Alonso, B.; Durand, J.-L.; Bujoli, B.; Gan, Z.; Hoatson, G. *Magn. Reson. Chem.* **2002**, *40*, 70.
(34) Desbiens, N.; Demachy, I.; Fuchs, A.; Kirsch-Rodeschini, H.; Soulard, M.; Patarin, J. *Angew. Chem., Int. Ed.* **2005**, *44*, 5310.
(35) Burneau, A.; Gallas, J.-P. In *The Surface Properties of Silicas*; Legrand, A. P., Ed.; John Wiley & Sons: Chichester, U.K., 1998; p 145.
(36) Trebosc, J.; Wiench, J. W.; Huh, S.; Lin, V. S.-Y.; Pruski, M. *J. Am. Chem. Soc.* **2005**, *127*, 3057.
(37) (a) d'Espinose de la Caillerie, J.-B.; Aimeur, M. R.; Kortobi, Y. E.; Legrand, A. P. *J. Colloid Interface Sci.* **1997**, *194*, 434. (b) Bronnimann, C. E.; Zeigler, R. C.; Maciel, G. E. *J. Am. Chem. Soc.* **1988**, *110*, 2023.

JP102663F